Path Loss Analysis Considering Atmospheric Refractivity and Precipitation for Air-to-Ground Radar

Sungsik Wang, *Senior Member, IEEE*, Tae Heung Lim, and Hosung Choo, *Member, IEEE*

***Abstract*—This letter reports a correlation analysis of path loss considering atmospheric refractivity and precipitation in an air-to-ground radar application. For the path loss estimation, the refractivity and rainfall attenuation models are derived using actual atmospheric data. The path loss along the range and altitude is obtained using parabolic equation software tool (PETOOL). The digital terrain elevation data (DTED) of the Suwon-Osan area, the radar antenna beam pattern, and environmental models are employed in the PETOOL. Then, we expand the path loss calculation in an azimuthal scan to observe the illuminated field intensity on the ground for a synthetic aperture radar (SAR) application. The results confirm that the illuminated field intensity for SAR applications is closely related to refractivity and precipitation.**

***Index Terms*—Correlation analysis, long-range air-to-ground propagation, path loss, precipitation, refractivity.**

I. Introduction

ADVANCES in radar technologies have led to significant improvements in the performance of long-range airborne radar systems, particularly for air-to-ground modes. An air-to-ground mode generally supports applications such as extracting synthetic aperture radar (SAR) images, detecting ground targets, and determining Doppler beam range [1]–[3]. In such applications, the wave propagation of the airborne radar system needs accurate on-target illumination to produce high-resolution images or precise target detections. However, wave propagations occasionally have severe attenuation due to external factors such as clutters, multipath interferences, wave refractions, and rainfall attenuations. In particular, it is considerably difficult to compute precise path losses when the airborne radar system is affected by the refractivity of an abnormal atmospheric environment and the attenuation of high precipitation. To overcome these problems, many studies on accurately estimating path loss considering atmospheric and weather conditions have used various propagation models, such as the ITU terrain model [4], the two-ray ground-reflection model [5], and the Egli model [6]. These investigations have achieved highly accurate path loss predictions considering only the single factor of refractivity or rainfall attenuation within the range of 50 km. However, an in-depth consideration of the relation between path loss and major environmental weather conditions, such as rainfall, and atmospheric refractivity is still needed.

In this letter, we propose a correlation analysis of path loss considering atmospheric refractivity and precipitation in air-to-ground radar applications. For the path loss estimation, the refractivity model is calculated using atmospheric data extracted from the Osan meteorological observatory in Korea [7]. Furthermore, the rainfall attenuation model is provided using the precipitation based on the P.530-17, P.837-7, and P.838-3 models [8]–[10]. Then, the path loss along the range and altitude for airborne radar wave propagation is calculated using parabolic equation MATLAB software tool (PETOOL) [11]. Herein, we employ the digital terrain elevation data (DTED) from the Suwon-Osan area, the radar antenna beam pattern, and the environmental models of specific cases in PETOOL [12]. To consider the detailed air-to-ground situation, the calculated path losses on the ground terrain are obtained for each case. We expand the path loss calculation in an azimuthal scan to observe the illuminated field intensity on the ground for an SAR application. Finally, the entire atmospheric data from 2016 to 2020 are used to evaluate path loss correlation with refractivity and precipitation. The results for the last five years show that path losses are closely related to refraction and precipitation.

II. Proposed Analysis

A. Path Loss Estimation Using Refractivity and Rainfall Attenuation Models

Fig. 1 shows a conceptual figure of an air-to-ground beam steering scenario for the field illumination intensity observations of wave propagation in accordance with weather conditions. An aircraft, located at a height (h_A) of 5 km, tilts the steering angle of the antenna toward the ground to observe the field illumination intensities of the wave propagation on ground terrains. The

Manuscript received May 3, 2021; revised July 2, 2021 and July 7, 2021; accepted July 8, 2021. Date of publication August 2, 2021; date of current version October 6, 2021. This work was supported in part by a grant-in-aid of HANWHA SYSTEMS, the Basic Science Research Program through the National Research Foundation of Korea (NRF) funded by the Ministry of Education under Grant NRF-2015R1A6A1A03031833, and in part by the National Research Foundation(NRF) the Korea Government under NRF Grant NRF-2017R1A5A1015596. *(Corresponding author: Tae Heung Lim.)*

The authors are with the School of Electronic and Electrical Engineering, Hongik University, Seoul 04066, South Korea (e-mail: kingwss@gmail.com; qpzm_0105@naver.com; hschoo@hongik.ac.kr).

Digital Object Identifier 10.1109/LAWP.2021.3101251

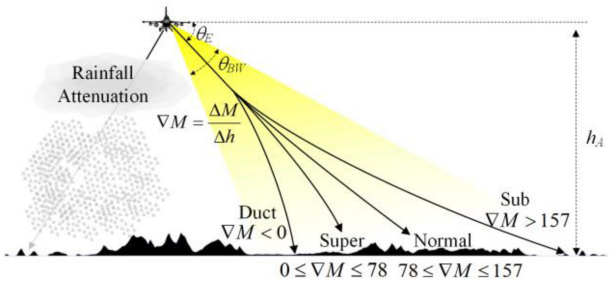

Fig. 1. Conceptual figure of an air-to-ground beam steering scenario of wave propagation in accordance with weather conditions.

antenna beam pattern operating at 10 GHz is steered with an elevation angle (θ_E) of 2.5°, which has a half-power beamwidth (θ_{BW}) of 2°. In the examination of wave propagation, it is important to consider external environmental factors, such as air temperature, air pressure, relative humidity, and precipitation, because these factors can cause serious wave refractions or attenuations of wave propagation. For wave refractions, it is essential to calculate the modified refractivity M along the altitude by using (1) and (2), as follows [13]:

$$N = \left(77.6 \times 10^{-6} \times \frac{P}{T} + 0.373 \times \frac{e}{T^2}\right) \times 10^6 \quad (1)$$

$$M = N + 0.157 \times h \quad (2)$$

where N is the refractive index, P is the air pressure in millibars, and e is the water vapor pressure in millibars. T is the absolute temperature in K, and h indicates the altitude in km. In fact, the gradient of modified refractivity ∇M according to the altitude is critical since the wave propagation direction is bent depending on ∇M. According to the levels of ∇M, the wave refraction can conventionally be divided into four types of refraction: normal, sub, super, and duct [13].

Fig. 2(a) represents the refractivity along the altitude in accordance with each wave refraction, where the solid, dashed, dotted, and dash-dotted lines indicate the actual refractivity on January 27 (sub), March 8 (normal), May 4 (super), and July 29 (duct) in 2020 for Cases 1-4, respectively. In addition, the attenuation of wave propagation occurs due to rainfall. The rainfall attenuation L_r according to the range can be calculated by the P.530-17, P.837-7, and P.838-3 models in terms of precipitation, as follows [8]–[10]:

$$L_r = \gamma_r d_{eff} \quad [\mathrm{dB}] \quad (3)$$

$$\gamma_r = \kappa \rho^{\alpha} \quad [\mathrm{dB/km}] \quad (4)$$

$$\mathrm{d_{eff}} = \frac{R_t}{0.477 R_t^{0.633} \rho_{0.01}^{0.0173\alpha} f^{0.123} - 10.579\left(1 - \exp\left\{-0.024 R_t\right\}\right)} \quad [\mathrm{km}] \quad (5)$$

where f is the frequency in GHz, γ_r is the specific rainfall attenuation in dB/km, and R_t is the target range in km. ρ is the rainfall precipitation in mm/h, and d_{eff} is the effective propagation distance. α and κ are the rainfall attenuation parameters depending on the frequency, polarization state, and angle of the signal path. Fig. 2(b) shows the rainfall attenuation according to the range in terms of precipitation. The solid, dashed, and dotted lines denote the average daily precipitations for Case 1 (1.4 mm/h) and Case 4 (87 mm/h), respectively. The maximum attenuation level is 2.4 dB for the low precipitation of Case 1; however, the attenuation dramatically increases to 42.8 dB for the hard rainfall weather in Case 4.

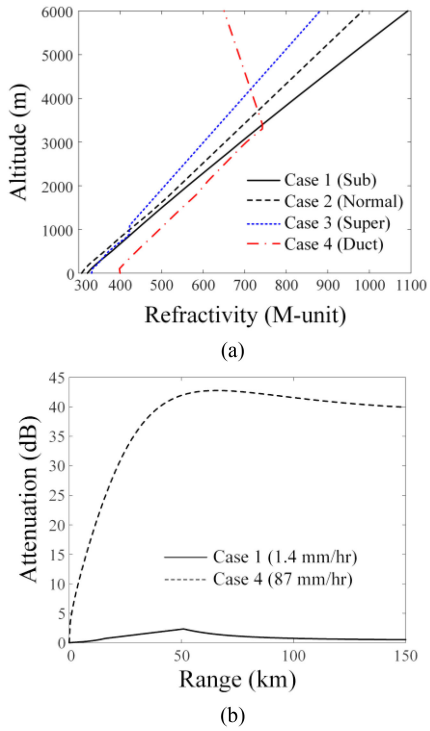

Fig. 2. Refractivity and attenuation models in terms of the atmospheric and weather conditions in the Suwan-Osan area. (a) Refractivity along the altitude for four cases. (b) Rainfall attenuation along the range for Cases 1 and 4.

To observe the field intensity of the wave propagation, we estimate the path loss levels using PETOOL software [11], where the DTED nearby Suwon-Osan in Korea, the beam steering pattern, the refractivity model, and the rainfall attenuation model are included as input parameters. Fig. 3(a) presents the path losses according to the range from 0 to 150 km considering the aforementioned refractivity and rainfall attenuation models for the four cases. These path losses are obtained at a height of 1.8 m from the terrain ground to observe the illuminated field intensity. For all cases, the low path loss levels are perceived in the range from 80 to 120 km because the range site is under the steered beam of the airborne radar. In this range, some drastically high path loss levels are also observed due to the shaded area of the terrain with the ground reflections. The average path losses in the steered beam region for Cases 1-3 are 168, 166, and 164.4 dB, respectively. In contrast, for Case 4, the average path loss level is 204 dB, which is dramatically higher than the

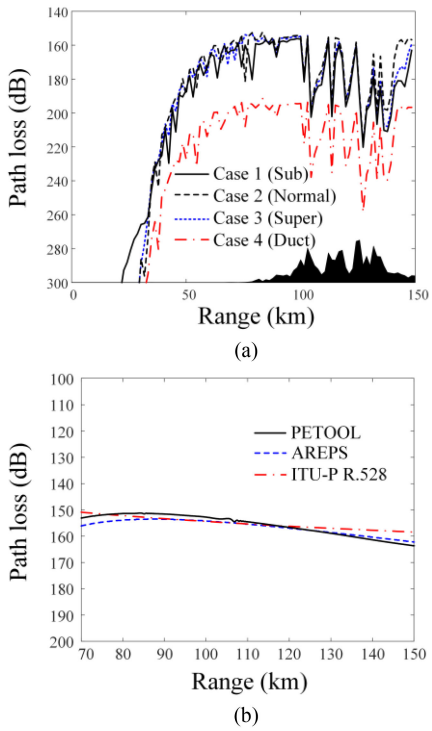

Fig. 3. Estimated path loss results along the range. (a) Considering the aforementioned refractivity and rainfall attenuation models for the four cases. (b) Simulation verification using AREPS software and the ITU-R. 528 model.

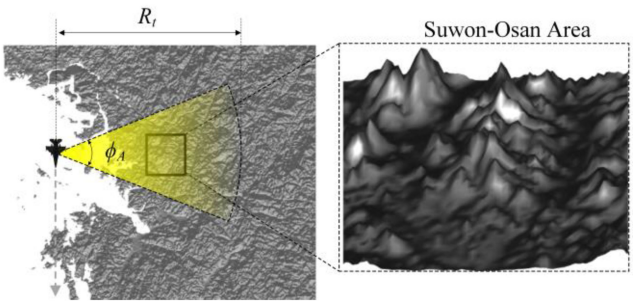

Fig. 4. Conceptual figure of a 2-D azimuthal scanning scenario.

other cases since the high precipitation leads to the considerable attenuation of the wave propagation. To verify these simulation results, we compare the path loss results using other propagation models such as AREPS software [14] and the ITU-R. 528 model [15], as shown in Fig. 3(b). The path losses are calculated on the assumption of normal atmospheric conditions with no precipitation, and the results demonstrate that all path losses agree well with each other.

B. 2-D Path Loss Estimation and Correlation With Atmospheric and Weather Conditions

Fig. 4 illustrates the conceptual figure of a two-dimensional (2-D) azimuthal scanning scenario to observe the field illumination on ground terrain for the SAR application. The aircraft

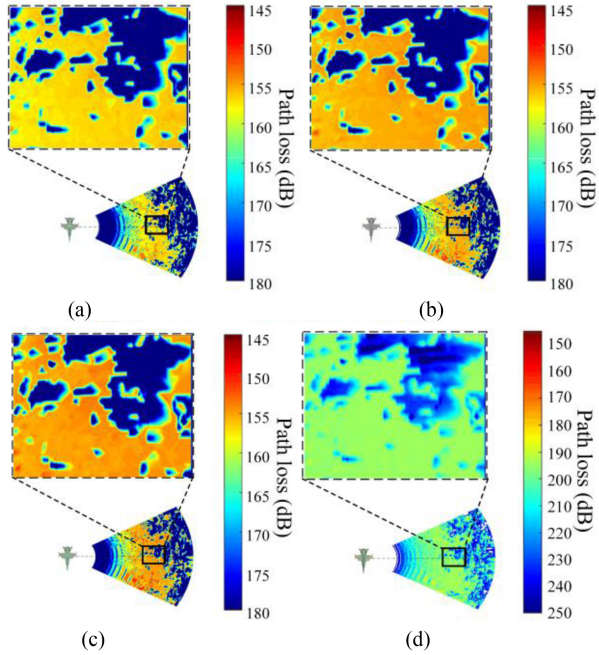

Fig. 5. 2-D regional path losses on the ground terrain in 2020. (a) Case 1 (Jan.27) (b) Case 2 (Mar.8) (c) Case 3 (May.4) (d) Case 4 (Jul.29).

operates a beam scanning in terms of ϕ_A to examine the field illumination intensity on the ground terrain in the Suwon-Osan area while flying along the West Sea in Korea. Fig. 5(a)-(d) presents the resulting 2-D regional path losses on the ground terrain, where red and blue blurs indicate the low and high path loss results. Cases 1 and 4 are the cases for rainfall, and the average path losses in the Suwon-Osan area for each case are 168.5 and 205.2 dB, respectively, as shown in Fig. 5(a) and (d). The results demonstrate that high precipitation induces a dramatic increase in path losses. For Cases 2 and 3, the average path losses are 166.7 and 165.4 dB, respectively. Note that refractivity also affects wave propagation in the air-to-ground situation, as shown in Fig. 5(b) and (c). In particular, the super refraction for Case 3 reduces the path loss because the wave bends toward the ground, making the beam more concentrated on the Suwon-Osan area compared to Case 2 (normal). To confirm the relation of path loss with refractivity and precipitation, we extract one year of atmospheric and precipitation data for 2020 from the Osan meteorological observatory and the path losses are calculated in terms of the whole weather and atmospheric data. Then, we also calculate the correlation between the path loss and the massive data to clarify the relationship between path loss and the weather environment. As a summary, the overall path loss analysis process is shown in Fig 6.

Fig. 7(a) represents the path loss results and precipitation according to rainy days in 2020, where the refractivity data in the rainy days are used for the path loss calculations. The black and red lines indicate the path loss and precipitation, respectively. In the Korean summer from June 1 to August 31,

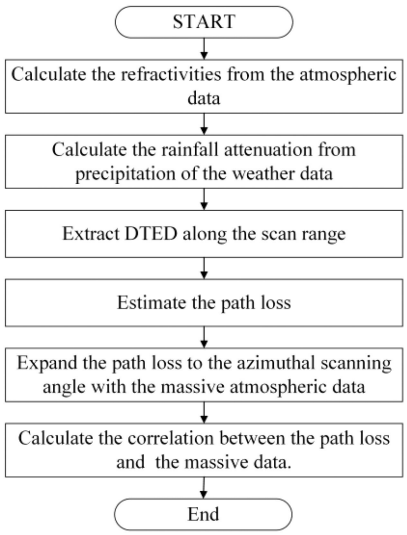

Fig. 6. Flowchart of the path loss analysis process.

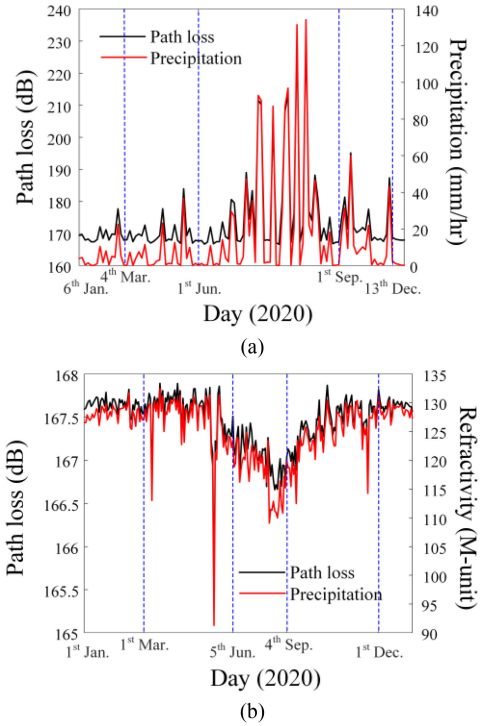

Fig. 7. Path loss results in the presence and absence of rainfall in 2020. (a) With the precipitation according to the rainy day. (b) With the average refractivity along altitude in 2020 except for the rainy day.

the path loss level particularly increases to 232.8 dB, and there is a precipitation of 134.2 mm/h due to the heavy rainfall during the rainy season. It is evident that the resulting path loss level follows the precipitation trends throughout the rainy day. In addition, we also achieve path loss results according to the average refractivity along altitude over one year, excluding rainy days, as presented in Fig. 7(b). Although the path loss level according to the refractivity does not change as much as the precipitation result, the tendency of the path loss graph over the date is extremely similar to that of the average refractivity. Therefore, we confirm that the path losses of the air-to-ground wave propagation are directly affected by refractivity and precipitation. To clarify the relationship between path loss and the weather environment, the correlation is calculated by utilizing a Pearson correlation coefficient between X and Y as follows [16]:

TABLE I
PATH LOSS CORRELATION COEFFICIENT

Year	Path loss correlation coefficient	
	Refractivity	Precipitation
2020	0.966892	0.998909
2019	0.831302	0.998893
2018	0.982798	0.999250
2017	0.829662	0.999105
2016	0.864828	0.999018

$$c_{XY} = \frac{N\sum x_i y_i - \sum x_i \sum y_i}{\sqrt{N\sum x_i^2 - \left(\sum x_i\right)^2}\sqrt{N\sum y_i^2 - \left(\sum y_i\right)^2}} \tag{6}$$

where x_i and y_i are sample components of X and Y with total N samples. X is the path loss result, and Y is the refractivity or the precipitation. The value of c_{XY} is in the range from -1 to 1. When c_{XY} is equal to 1 or -1, X and Y have a completely positive or negative correlation. However, when c_{XY} is equal to 0, X, and Y are absolutely not correlated. The correlation coefficients of the path loss with refractivity and precipitation in 2020 are 0.967 and 0.999, respectively, and the results numerically explain that the path loss trends follow refractivity and precipitation. To confirm these trends, the correlation coefficients are calculated using massive atmospheric data from 2016 to 2020, and the detailed values are listed in Table I.

III. CONCLUSION

We have investigated the novel correlation analysis of path loss considering atmospheric refractivity and precipitation in air-to-ground radar applications. To predict the illuminated field in airborne radar wave propagation, the path loss on the ground terrain was extracted with the refractivity model and the rainfall attenuation model. The 2-D illuminated field intensity scenario was computed for an SAR application including the DTED of the Suwon-Osan area, the radar antenna beam pattern, and the environmental models. The resulting average path losses in the Suwon-Osan area for Cases 1-4 were 168.5, 166.7, 165.4, and 205.2 dB, respectively. In addition, the correlation coefficients of the path loss with refractivity and precipitation in 2020 were 0.967 and 0.999, respectively. The results demonstrated that the illuminated field intensity for an SAR application was closely correlated with refractivity and precipitation.

REFERENCES

[1] J.-H. Lim *et al.*, "Performance evaluation of a modified SweepSAR mode for quad-pol application in SAR systems," *J. Electromagn. Eng. Sci.*, vol. 20, no. 3, pp. 199–206, Jul. 2020.

[2] J.-H. Nam, J.-W. Rim, H. Lee, I.-S. Koh, and J.-H. Song, "Modeling of monopulse radar signals reflected from ground clutter in a time domain considering doppler effects," *J. Electromagn. Eng. Sci.*, vol. 20, no. 3, pp. 190–198, Jul. 2020.

[3] E. H. Kim and J. Park, "Dwell time optimization of alert-confirm detection for active phased array radars," *J. Electromagn. Eng. Sci.*, vol. 19, no. 2, pp. 107–114, Apr. 2019.

[4] Recommendation ITU-R P.2041, "Prediction of path attenuation on links between an airborne platform and space and between an airborne platform and the surface of the earth," International Telecommunication Union, Geneva, Switzerland, 2013.

[5] S. Loyka and A. Kouki, "Using two ray multipath model for microwave link budget analysis," *IEEE Antennas Propag. Mag.*, vol. 43, no. 5, pp. 31–36, Oct. 2001.

[6] J. J. Egli, "Radio propagation above 40 MC over irregular terrain," *Proc. IRE*, vol. 45, no. 10, pp. 1383–1391, Oct. 1957.

[7] "Korea Meteorological Administration," Korea, 2021. [Online]. Available: https://www.kma.go.kr/eng/index.jsp

[8] Recommendation ITU-R P.530-17, "Propagation data and prediction methods required for the design of terrestrial line-of-sight systems," International Telecommunication Union, Geneva, Switzerland, 2017.

[9] Recommendation ITU-R P.837-7, "Characteristics of precipitation for propagation modelling," International Telecommunication Union, Geneva, Switzerland, 2017.

[10] Recommendation ITU-R P.838-3, "Specific attenuation model for rain for use in prediction methods," International Telecommunication Union, Geneva, Switzerland, 2005.

[11] O. Ozgun, G. Apaydin, M. Kuzuoglu, and L. Sevgi, "PETOOL: MATLAB-based one-way and two-way split-step parabolic equation tool for radiowave propagation over variable terrain," *Comput. Phys. Commun.*, vol. 182, no. 12, pp. 2638–2654, Dec. 2011.

[12] "National Geographic Information Institute," Korea, 2018. [Online]. Available: https://www.ngii.go.kr/eng/main.do?

[13] Recommendation ITU-R P.453-14, "The radio refractive index: Its formula and refractivity data," International Telecommunication Union, Geneva, Switzerland, 2017.

[14] *User Manual for Advanced Refractive Effects Prediction System (AREPS)*. San Diego, CA, USA: Space Naval Warfare System Center, 2004.

[15] Recommendation ITU-R P.528-4, "A propagation prediction method for aeronautical mobile and radionavigation services using the VHF, UHF and SHF bands," International Telecommunication Union, Geneva, Switzerland, 2019.

[16] X. Sun, Z. Shi, G. Lei, Y. Guo, and J. Zhu, "Multi-Objective design optimization of an IPMSM based on multilevel strategy," *IEEE Trans. Ind. Electron.*, vol. 68, no. 1, pp. 139–148, Jan. 2020.